IEEE Photonics Journal
An IEEE Photonics Society Publication

Ultracompact On-Chip Multiplexed Sensor Array Based on Dense Integration of Flexible 1-D Photonic Crystal Nanobeam Cavity With Large Free Spectral Range and High *Q*-Factor

Volume 9, Number 4, August 2017

Daquan Yang
Bo Wang
Xin Chen
Chuan Wang
Yuefeng Ji

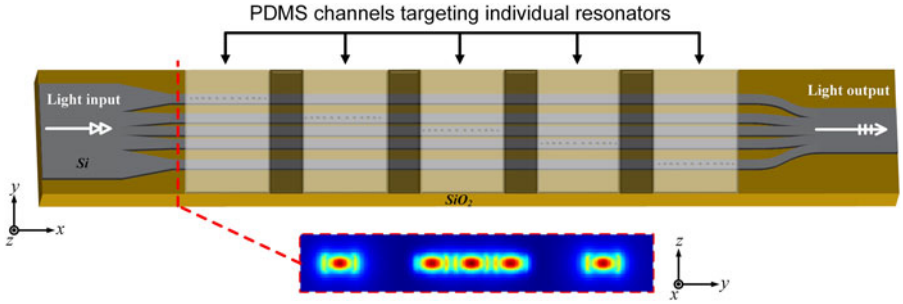

DOI: 10.1109/JPHOT.2017.2710136
1943-0655 © 2017 IEEE

Ultracompact On-Chip Multiplexed Sensor Array Based on Dense Integration of Flexible 1-D Photonic Crystal Nanobeam Cavity With Large Free Spectral Range and High *Q*-Factor

Daquan Yang,[1] Bo Wang,[1] Xin Chen,[1] Chuan Wang,[2] and Yuefeng Ji[1]

[1]State Key Laboratory of Information Photonics and Optical Communications, School of Information and Communication Engineering, Beijing University of Posts and Telecommunications, Beijing 100876, China
[2]State Key Laboratory of Information Photonics and Optical Communications, Beijing University of Posts and Telecommunications, Beijing 100876, China

DOI:10.1109/JPHOT.2017.2710136

Manuscript received May 5, 2017; revised May 25, 2017; accepted May 26, 2017. Date of publication June 2, 2017; date of current version June 29, 2017. This work was supported in part by the Natural National Science Foundation of China under Grants 61501053, 61471050, and 61372118 and in part by the State Key Laboratory of Information Photonics and Optical Communications, China. Corresponding author: D. Yang (e-mail: yangdq5896@163.com).

Abstract: A method for the dense integration of one-dimensional (1-D) photonic crystal nanobeam cavity (PCNC) based integrated sensor array (1-D-PCNC-ISA) is proposed. The 1-D-PCNC-ISA consists of multiple parallel-connected sensing channels with airgap separations. On each channel, only a single flexible 1-D-PCNC sensor with large free spectral range (FSR) and high Q-factor is contained. With proper engineering of the FSR, multiple ultracompact high-sensitivity 1-D-PCNC sensors can be integrated into microarrays without resonance overlap, and be interrogated simultaneously between a single input/output ports. Using 3-D finite-difference-time-domain (3-D-FDTD) method, the performance of the device is investigated theoretically in the whole paper. With optimization design, a large FSR as wide as 197 nm and high Q-factor $\sim 2 \times 10^5$ can be achieved. Moreover, the refractive index sensitivities of a 5-channel 1-D-PCNC-ISA as high as 170.6, 152.7, 138.5, 128.1, and 120.5 nm/RIU are obtained. Particularly, the footprint of a 5-channel 1-D-PCNC-ISA is $\sim 7\,\mu$m $\times$ 65 μm (width by length), which is decreased by three orders of magnitude compared to the sensor arrays based on 2-D-PC cavity platforms. To the best of our knowledge, this is for the first time that a 1-D-PCNC based multichannel parallel-connected sensor array has been displayed with channel spacing as small as 0.195 μm, extinction ratio $>$ 20 dB and Q-factor $> 10^5$, respectively, without using particular materials or complexities in fabrication. Both the specific result and the general idea are promising in future ultracompact lab-on-a-chip applications and nanophotonic integrations.

Index Terms: Optical interconnects, Photonic crystals, Nanocavities, Sensors, Silicon nanophotonics, Integrated nanophotonic systems

1. Introduction

Multiplexed sensor arrays permit simultaneous detection of many binding interactions with specific immobilized antibodies from the same bio-sample at the same instant of time. Over the past decades, compact, sensitive, and low-cost integrated sensor array (ISA) structures are of great interest for lab-on-a-chip multiplexed sensing applications [1]–[5]. Integrated photonic resonators and optical micro-cavities [6] offer a viable solution for monolithic lab-on-chip sensing due to their compactness, scalability, and high sensitivity. So far, various different integrated photonic resonators and optical micro-cavities with multiple resonant modes have been developed as optical sensor arrays. The most exploited schemes are based on the principles of whispering-gallery mode (WGM) resonator [7], [8], Mach-Zehnder interferometer (MZI) [9], surface plasmon resonator (SPR) [10]–[13], ring resonator (RR) [14]–[22], fiber Bragg grating (FBG) [23]–[33], photonic crystals fiber (PCF) [34], [35], photonic crystals waveguide (PCW) [36], [37] and photonic crystals cavity (PCC) [38]–[52]. Particularly among these, the ultra-compact size, low mode volume (V_m), high quality factor (Q), high refractive index (RI) sensitivity (S), and relatively simple geometry of compact PCC, makes them a suitable option for on-chip density-integrated sensor array devices as compared to other alternatives. However, most of PCC-based integrated sensor arrays (PCC-ISA) mentioned above [38]–[51] are based on two dimensional photonic crystal cavity (2D-PCC) platforms. The footprints of these 2D-PCC based integrated sensor arrays (2D-PCC-ISAs) are usually too large, which are not suitable for on-chip ultra-high density integration. Example of such system include that Yan *et al*. who demonstrated a 2-channel 2D-PCC-ISA formed by series-connected PCW and PCC based sensor [49]. The footprint of the full 2-channel 2D-PCC-ISA device is $\sim 50\,\mu$m $\times$ 2000 μm in [49]. In addition, these 2D-PCC-ISAs mentioned above are not suitable for high-yield large-scale manufacturing and high integrability with optical waveguides and circuits.

Compared to 2D-PCC-ISAs above, one-dimensional (1D) PC nanobeam cavity based integrated sensor arrays (1D-PCNC-ISAs) have been developed and demonstrated as a promising platform for nanoscale high density-integrated sensor array devices with high sensitivity and multiplexed detection capability [52], due to their ultra-small size, ultra-low mode volume, and high integrability with optical waveguides and photonic integrated circuits (PICs) [53], [54]. For example, Mandal *et al*. demonstrated a nanoscale multi-channel opto-fluidic sensor array based on a silicon waveguide with a side-coupled 1D-PCNC array that lies adjacent to a silicon-bus-waveguide [52]. However, the extinction ratio of single drop of the demonstrated 1D-PCNC-ISA in [52] is lower than 10 dB. Moreover, the presented multi-channel 1D-PCNC-ISA need multiple coupling optical fibers to detect the output responses from all 1D-PCNC sensor units simultaneously, which cannot be interrogated simultaneously with a single input and output, making the packaging and alignment to be fragile and cost-expensive.

From the practical application perspective, when designing a portable on-chip nanoscale integrated sensor array device, ideally one would like an architecture needs to maximize the number of sensing units which can be interrogated simultaneously between a single input optical fiber and a single output optical fiber, making the devices packing and alignment robust and cost-effective. Towards this direction, in this paper, based on wavelength domain multiplexing (WDM) technique [55] we propose a novel paradigm to multiplex multiple 1D PC nanobeam cavity sensors (1D-PCNCSs) between a single input port and a single output port. The proposed 1D-PCNCSs based integrated sensor array (1D-PCNC-ISA) architecture is formed by multiple parallel-connected channels of 1D-PCNCS with gap separations. On each channel, only a single flexible 1D photonic crystal nanobeam cavity (1D-PCNC) with large free spectral range (FSR) and high Q-factor is contained. With proper engineering of the FSR of 1D-PCNC on each channel, multiple high sensitivity 1D-PCNC sensors can be integrated into microarrays without resonance overlap. Herein, to analyze the performance of the proposed multi-channel 1D-PCNC-ISA, the concept model of a 5-channel 1D-PCNC-ISA is presented. All channels are connected in parallel. And the channel spacing between adjacent channels as small as 0.195 μm can be achieved. To enable all sensors on each channel to be interrogated simultaneously with a single input and output, a 1 $\times$ 5 taper-type equal power splitter and a 5 $\times$ 1 S-type power combiner are used in the input port and output port, respec-

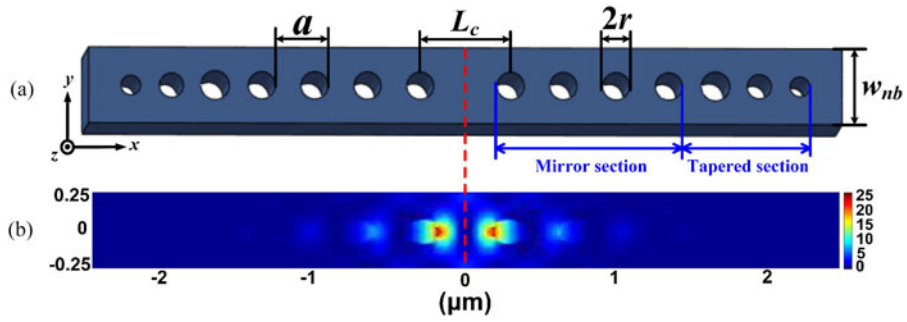

Fig. 1. (a) Schematic of the designed 1D-PCNC. The structure is symmetric with respect to its center (red dashed line). (b) 3D-FDTD simulation of major field distribution profile ($|Ey|$) of a specific targeted resonant mode ($\sim$1367 nm) for sensing purpose. Here, in the mirror section of 1D-PCNC, the number of the air-hole gratings $N_m = 4$, all the air-hole gratings radii are kept same as $r = 85$ nm and periodicity $a = 350$ nm. In the tapered section of 1D-PCNC, the number of the air-hole gratings $N_t = 3$, the air-hole gratings radii are linearly decreased from inside to outside as 95 nm, 80 nm, and 65 nm, respectively; and the periodicities are linearly decreased from inside to outside as 310 nm, 290 nm, and 270 nm, respectively. The width and thickness of the silicon nanobeam waveguide are $w_{nb} = 500$ nm and $h = 220$ nm. $n_{air} = 1.0$ and $n_{si} = 3.46$ The unit of the x/y axis is micrometers.

tively. With three-dimensional finite-difference time-domain (3D-FDTD) method, the performance of the presented sensor array device is investigated theoretically. With optimization design, the large FSR 200 nm and high Q-factor $\sim 2 \times 10^5$ of 1D-PCNC can be achieved, respectively. The extinction ratio of well-defined resonance peak for sensing purpose exceeds 20 dB. The calculated bulk RI sensitivities of the presented 5-channel 1D-PCNC-ISA as high as 170.6 nm/RIU, 152.7 nm/RIU, 138.5 nm/RIU, 128.1 nm/RIU, and 120.5 nm/RIU are obtained (RIU = Refractive Index Unit). Moreover, the footprint of the proposed 5-channel 1D-PCNC-ISA is as small as $\sim 7\,\mu$m $\times$ 65 μ m (width by length), which is decreased by three orders of magnitude compared to the sensor arrays based on 2D-PC cavity platforms [41]–[50], without any lowering of RI-sensitivities and Q-factors.

2. Design Ultra-Compact 1-D PC Nanobeam Cavity (1-D-PCNC) With High Q-factor and Large Free Spectral Range (FSR)

Fig. 1(a) shows the schematic of the proposed 1D PC nanobeam cavity (1D-PCNC) design, inspired by [56], which consists of a single row of air-hole gratings embedded in a nanobeam waveguide based on silicon-on-insulator (SOI) material. The RI of air-hole gratings and silicon waveguide are $n_{air} = 1.0$ and $n_{si} = 3.46$, respectively. The width and thickness of the silicon nanobeam waveguide are $w_{nb} = 500$ nm and $h = 220$ nm, respectively. As seen, the proposed 1D-PCNC structure, which is symmetric with its center (red dashed line), consists of a waveguide region of length L_c (defined as cavity length, namely the distance between the two adjacent air holes in the cavity center) that supports propagating modes, bounded on each side by a finitely long modulated Bragg mirror. Here, the modulated Bragg mirror on each side consists of two sections: (i) Mirror section and (ii) Tapered section, respectively. In the Mirror section, all the air-hole gratings radii (r) and periodicities (a) are kept fixed. In the Tapered section, the air-hole gratings radii and periodicities are linearly decreased from inside to outside, respectively. The design of gradually tapered hole structure is based on mode matching [57], [58], which produces a significantly enhanced Q-factor and optical transmission through reductions in propagation losses and scattering that occur locally at transitions between the mirror section and tapered section of the cavity. Without loss of generality, a TE-like cavity mode is considered. By using 3D-FDTD method [59], Fig. 1(b) shows the major field distribution profile ($|Ey|$) in x-y plane of the targeted resonant mode for sensing purpose. As seen, a significant amount of electric field is strongly localized within the cavity center, which makes the light-matter interactions enhanced to achieve high sensitive sensing.

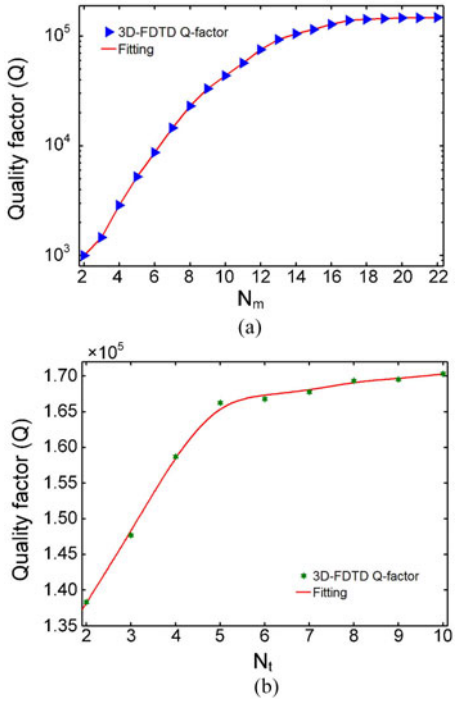

Fig. 2. 3D-FDTD calculated Q-factors as a function of (a) the number of the air-hole gratings (Nm) in the Mirror section changed from $N_m = 2$ to $N_m = 22$, while the number of the air-hole gratings (N_t) in the Tapered section is kept fixed as $N_t = 3$; and (b) the number of the air-hole gratings (N_t) in the Tapered section changed from $N_t = 2$ to $N_t = 10$, while the number of the air-hole gratings (N_m) in the Mirror section is kept fixed as $N_m = 21$.

Firstly, in order to design 1D PC nanobeam cavity (1D-PCNC) achieving high Q-factor, the number of the air-hole gratings (N_m) in the Mirror section and the number of the air-hole gratings (N_t) in the Tapered section are investigated in detail, respectively, when the cavity length $L_c = 375$ nm, the air-hole gratings radii and periodicities in Mirror section are kept fixed as $r = 85$ nm, $a = 350$ nm, respectively; the air-hole gratings radii and periodicities in Tapered section are linearly decreased from 95 nm to 65 nm, and from 310 nm to 270 nm, respectively. The width and thickness of the silicon nanobeam waveguide are kept fixed as $w_{nb} = 500$ nm and $h = 220$ nm, respectively. By using 3D-FDTD method, Fig. 2(a) shows the theoretical calculated Q-factors as a function of the number of the air-hole gratings (N_m) in the Mirror section changed from $N_m = 2$ to $N_m = 22$, while the number of the air-hole gratings (N_t) in the Tapered section is kept fixed as $N_t = 3$. As seen, as N_m increases, the Q-factor value increases. When N_m increases from $N_m = 2$ to $N_m = 17$, the cavity Q-factor sharply increases by two orders of magnitude, but when N_m increases larger than 18 ($N_m \geq 18$), it becomes smooth. The optimized Q-factor over 1.5×10^5 can be achieved. Fig. 2(b) shows the theoretical calculated Q-factors as a function of the number of the air-hole gratings (N_t) in the Tapered section changed from $N_t = 2$ to $N_t = 10$, while the number of the air-hole gratings (N_m) in the Mirror section is kept fixed as $N_m = 21$. As seen, as N_t increases, the Q-factor value also increases, but the magnitude is not large. And a slight increase is observed form 1.38×10^5 to 1.71×10^5.

Next, in order to further design 1D PC nanobeam cavity (1D-PCNC) having large FSR, the cavity FSR and resonant wavelength in terms of the cavity length (L_c) are discussed in detail. Herein, in order to save the simulation time of the transmission calculation, we used a high transmission but low Q-factor geometry: the number of the air-hole gratings in the Mirror section (N_m) and in the tapered section (N_t) are chosen to be $N_m = 4$ and $N_t = 3$, respectively. With 3D-FDTD simulation, we obtained the transmission of the 1D-PCNC, as light is launched from the input bus waveguide

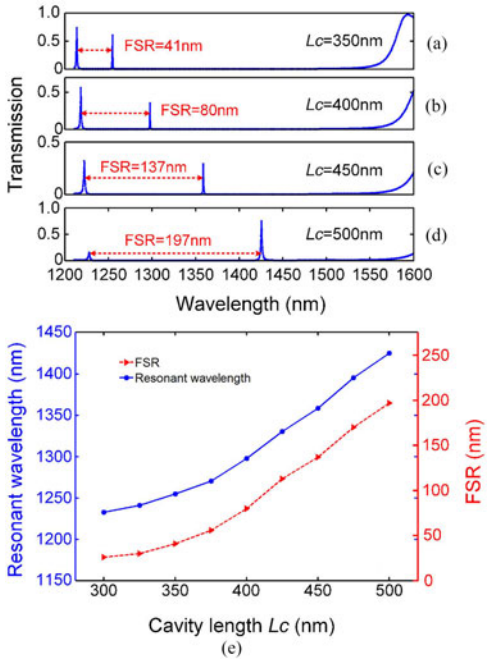

Fig. 3. (a)-(d) 3D-FDTD composed transmission spectra when the cavity length $L_c = 350$ nm, 400 nm, 450 nm and 500 nm, respectively. (e) Cavity resonant wavelength and FSR as a function of the cavity length (L_c) changed from $L_c = 300$ nm to $L_c = 500$ nm, where $N_m = 4$, $N_t = 3$. The air-hole gratings radii and periodicities in the Mirror section and the Tapered section are kept fixed.

(fundamental TE-like mode) and collected from the output bus waveguide. Fig. 3(a)–(d) show the composed transmission spectra when the cavity length $L_c = 350$ nm, 400 nm, 450 nm and 500 nm, respectively. As seen, with proper engineering of the cavity length (L_c) of 1D-PCNC, an arbitrary wide FSR can be obtained, indicating that multiple 1D-PCNC sensors can be connected in parallel without resonance overlap. Fig. 3(e) shows the cavity FSR and resonance wavelength as a function of the cavity length (L_c) changed from $L_c = 300$ nm to $L_c = 500$ nm. As expected, with the cavity length increased, the cavity resonant wavelength moves towards longer wavelength, due to the increase in high-dielectric material in the cavity center region [60]. As seen, the cavity FSR increases with the increasing cavity length. When the cavity length $L_c = 500$ nm, the cavity FSR as large as 197 nm can be achieved, which is wide enough for multiplexed sensing applications compared to the previous works [61]–[63]. In addition, the footprint of the proposed 1D-PCNC is ultra-compact as small as $\sim 0.5\,\mu$m $\times$ $4.0\,\mu$m (width by length, with $L_c = 500$ nm, $N_m = 4$, and $N_t = 3$ shown in Fig. 1(a). Thus, the proposed ultra-compact 1D-PCNC with large FSR is potentially a promising platform for high-density integrated sensor array design and lab-on-chip multiplexed sensing applications.

3. Design Ultra-Compact On-Chip Multiplexed Sensor Array Based on Dense Integration of 1-D Photonic Crystal Nanobeam Cavity

Herein, based on the proposed ultra-compact 1D PC nanobeam cavity (1D-PCNC) with high Q-factor and large FSR mentioned above, an ultra-compact on-chip multiplexed sensor array is proposed in the upper 220-nm-thick silicon layer of a silicon-on-insulator (SOI) substrate. Since the suspended 1D PC nanobeam membrane structures are fragile and difficult to any sort of post processing to enable multiplexed sensing experiments of individual targets, the proposed 1D-PCNC based integrated sensor array (1D-PCNC-ISA) is design with silica substrate to enhance the device robustness. The device consists of multiple parallel-connected channels of 1D-PCNC with gap sep-

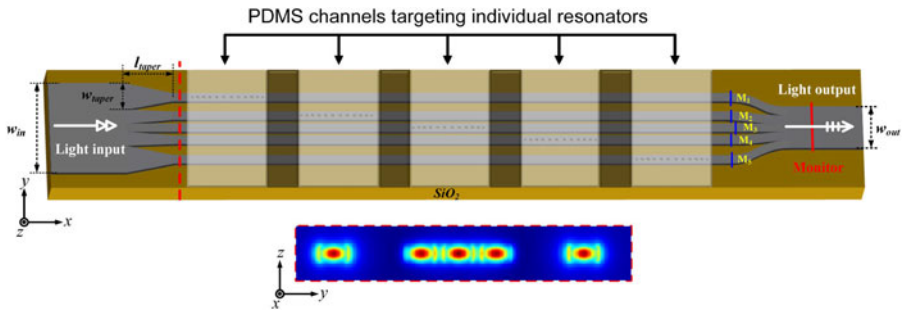

Fig. 4. Schematic of the proposed 5-parallel-channel 1D-PCNC-ISA with single input port and output port. For each channel, only a single 1D-PCNC sensor is consisted. In the input port and output port, a 1×5 taper-type equal power splitter and a 5×1 S-type power combiner are used to split and combine the waveguides, respectively. The footprint of the whole 5-parallel-channel 1D-PCNC-ISA, including the input bus waveguide and output bus waveguide, is as small as $\sim 7\,\mu$m $\times$ 65 μm (width by length).The inset below is the cross-section of electric field profile for the fundamental TE-like mode propagating through the splitter in *y*-*z* plane (transversal surface at the red dashed line).

arations. On each channel, via flexibly and carefully designing the cavity length (L_c) of 1D-PCNC, a transmission with a controllable FSR is obtained, containing the resonances of the 1D-PCNC for sensing purpose. With proper engineering of the FSR on each channel, multiple ultra-compact high sensitivity 1D-PCNC sensors can be integrated into microarrays without resonance overlap. In this work, to analyze the performance of the proposed multi-channel 1D-PCNC-ISA, the concept model of a 5-channel 1D-PCNC-ISA is presented, as shown in Fig. 4. As seen, all channels are connected in parallel. The adjacent channels are separated with air-gap separations, and the gap size between the two adjacent channels are 1.08 μm, 0.195 μm, 0.195 μm, and 1.08 μm (from top to bottom in the *y*-direction), respectively. To enable all 1D-PCNC sensors (1D-PCNCSs) on each channel to be interrogated simultaneously between a single input optical fiber and a single output optical fiber, a 1×5 taper-type equal power splitter and a 5×1 S-type power combiner, inspired by [64]–[66], are used in the input port and output port, respectively. In the input port, the displayed 1×5 taper-type equal power splitter consists of a silicon bus waveguide with width $w_{in} = 7\,\mu$m, and five taper-type branches connecting to a 5-channel 1D-PCNC-ISA. To achieve 5-way equal power division as possible, the width of both the first branch (B_1) and the fifth branch (B_5) is tapered from 2.45 μm to 0.5 μm, the width of both the second branch (B_2) and the fourth branch (B_4) is tapered from 0.71 μm to 0.5 μm, and the width of the third branch (B_3) is tapered from 0.68 μm to 0.5 μm. B_1, B_2, B_3, B_4, and B_5 refer to taper-type branches 1, 2, 3, 4, and 5 respectively, being 1 the branch on the top and 5 the branch at the bottom (in the *y*-direction). The length of each branch of the splitter is same as $l_{taper} = 10\,\mu$m. In the output port, the displayed 5×1 S-type power combiner consists of five S-type silicon waveguides and a bus waveguide with width $w_{out} = 2.5\,\mu$m. Between the power splitter and combiner, five 1D-PCNC sensor channels are connected in parallel. For all of the five channels, the number of the air-hole gratings (N_m) in the Mirror section and the number of the air-hole gratings (N_t) in the Tapered section of 1D-PCNC sensor are same as $N_m = 4$ and $N_t = 3$, respectively. The air-hole gratings radii in the Tapered section are linearly decreased from inside to outside as 95 nm, 80 nm, and 65 nm, respectively; and the periodicities in the Tapered section are linearly decreased from inside to outside as 310 nm, 290 nm, and 270 nm, respectively. However, in order to make the parallel connected 1D-PCNC-ISA without resonance overlap in the output transmission spectrum, the cavity length (L_c) of 1D-PCNC sensor on each channel are carefully and flexibly designed to obtain multiple different resonances for multiplexed sensing application. As shown in Fig. 4, the specific structural parameters of the proposed 1D-PCNC sensors on each channel are set as follows: (i) for the first channel: $L_c = 350$ nm, $a = 350$ nm, $r = 75$ nm. (ii) for the second channel: $L_c = 375$ nm, $a = 350$ nm, $r = 75$ nm. (iii) for the third channel: $L_c = 400$ nm, $a = 350$ nm, $r = 75$ nm. (iv) for the fourth channel: $L_c = 450$ nm, $a = 350$ nm, $r = 75$ nm. (v) for the fifth channel: $L_c = 475$ nm, $a = 350$ nm, $r = 75$ nm.

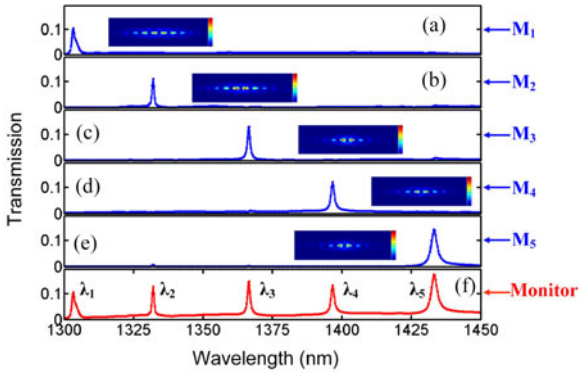

Fig. 5. (a)-(e) 3D-FDTD calculated transmission spectra obtained from each separated channel detected by the monitor M_1, M_2, M_3, M_4 and M_5, respectively. (f) 3D-FDTD output transmission spectrum of the proposed 5-channel 1D-PCNC-ISA, detected by the monitor set at the output port. Five separated resonances (λ_1, λ_2, λ_3, λ_4, and λ_5) at different wavelength positions (1303 nm, 1332 nm, 1367 nm, 1397 nm, and 1433 nm) without overlap are observed, respectively, when five 1D-PCNC sensors are connected in parallel. Inset are the major field distribution profile ($|Ey|$) in x-y plane of the observed targeted mode with the resonance wavelength at λ_1, λ_2, λ_3, λ_4, and λ_5, respectively.

With 3D-FDTD simulation, we obtained the transmission spectrum for each channel of the proposed parallel-connected 5-channel 1D-PCNC-ISA, as light is launched from the input bus waveguide (fundamental TE-like mode) coupled into the 1D-PCNC sensors by the above-designed coupler and finally collected from the output bus waveguide. For each channel, the total transmission spectra ranging from 1300 nm to 1450 nm detected by the monitor M_1, M_2, M_3, M_4 and M_5 are shown in Fig. 5(a)–(e), respectively. As seen, for each separated channel, there is only a single resonant mode observed in the transmission spectrum. Moreover, these resonant modes are observed at different wavelength positions. This indicates that multiple channels of 1D-PCNC sensors can be connected in parallel without resonance overlap, as displayed in Fig. 5(f). Fig. 5(f) presents the output transmission spectrum of the proposed 5-channel 1D-PCNC-ISA, detected by the monitor set at the output port. As expected, five separated resonances (λ_1, λ_2, λ_3, λ_4, and λ_5) at different wavelength positions (1303 nm, 1332 nm, 1367 nm, 1397 nm, and 1433 nm) without overlap are observed, respectively, when five 1D-PCNC sensors are connected in parallel. In addition, the extinction ratio of well-defined resonance peak for sensing purpose exceeds 20 dB, improved more than 10 dB compared to the sensor array device demonstrated in [52].

To verify the performance and the independence of the sensor units when they are connected in parallel, each sensor unit is independently subjected to the RI changes. Microfluidic channels architecture, which is fabricated using a soft lithography technique with polydimethylsiloxane (PDMS) [67], can be used to separate analytes for multiplexed sensing and make the RI of individual channels change separately during the experiment. The PDMS microfluidic channels are then bonded irreversibly to the chip with the channels running orthogonal to the 1D PC waveguide, with each channel aligned to one of the side resonators along the waveguide, as displayed in Fig. 4. Precise alignment of the channels with the resonators during bonding can be ensured by using a modified overhead optical microscope setup [52]. Here in, the multiplexed sensing performance of the proposed 5-channel 1D-PCNC-ISA device is investigated theoretically in detail. By using 3D-FDTD method, Fig. 6(a) and (b) shows the composed transmission spectra of the proposed 5-channel 1D-PCNC-ISA when only the sensor unit (S_1) and sensor unit (S_3) are subjected to RI variations, respectively, while the other sensor units are not. As seen, the wavelength shift in only one resonant mode used for sensing purpose is evident, and the other resonant modes do not shift. This means that these five resonant modes observed in the output transmission of the proposed 5-channel 1D-PCNC-ISA are independent of each other. In addition, multiple different targets can be detected independently at the same time in this parallel scheme. Thus, the multiplexing of the proposed sensors is quite straightforward given the fact that, when n sensors are placed in parallel, n resonant

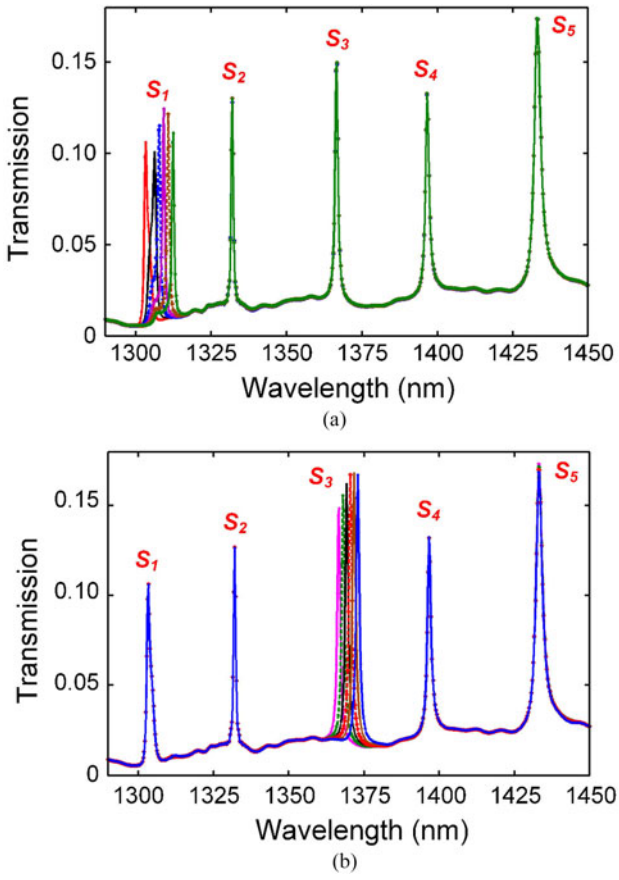

Fig. 6. 3D-FDTD composed transmission spectra observed when five sensor units are set in parallel and one of them (a) the sensor unit (S_1), and (b) the sensor unit (S_3) are under RI changes, respectively, and the others are not.

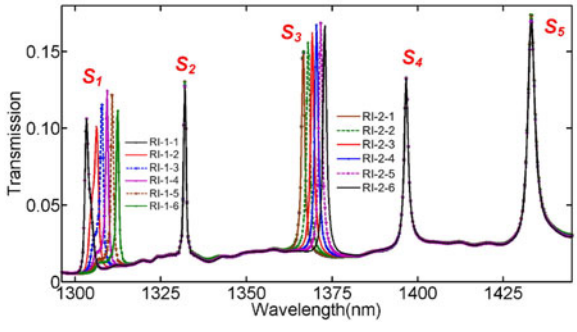

Fig. 7. 3D-FDTD composed transmission spectra observed when five sensing channels are set in parallel and two of them the first channel of sensor-1 (S_1), and the third channel of sensor-3 (S_3) are independently subjected to RI changes and the others are not.

modes are observed in the transmission. The proposed ultra-compact multi-channel 1D-PCNC-ISA in this paper is potentially an ideal platform for RI based multiplexed sensing.

In fact, the parallel multiplexed use is critical when each channel can be separately functionalized to respond to a certain perturbation or binding event. Fig. 7 shows the composed transmission spectra of the proposed 5-channel 1D-PCNC-ISA when five sensing channels are set in parallel and two of them (i) the first channel of sensor-1 (S_1), and (ii) the third channel of sensor-3 (S_3)

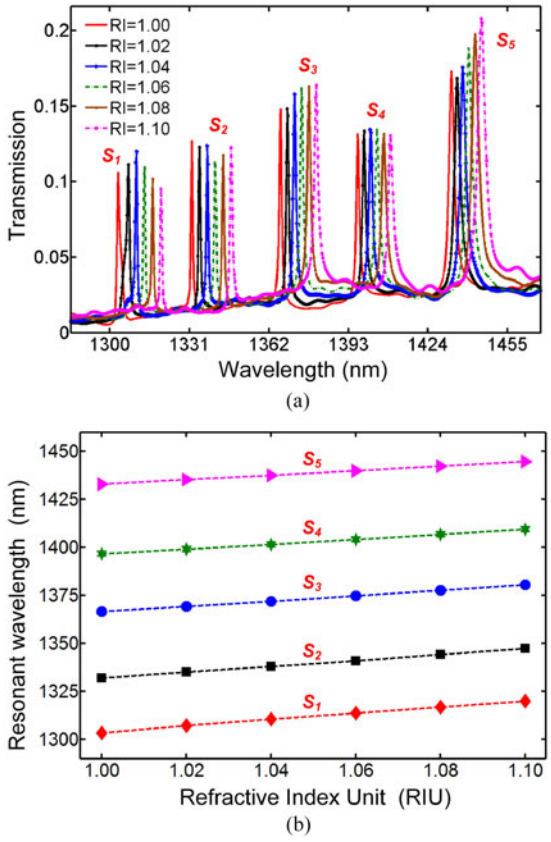

Fig. 8. (a) 3D-FDTD composed transmission spectra detected from the output port of the proposed 5-channel 1D-PCNC-ISA when all parallel-connected sensing channels are interrogated simultaneously under RI variations between a single input and output. The RI changes from RI = 1.00 to RI = 1.10. (b) The observed resonant wavelength shifts as a function of the RI variations in the five parallel-connected sensors.

are independently subjected to different RI changes, respectively, and other sensors are not. As seen, the targeted resonance modes of interest in each of the parallel channels are affected by the RI changes independently. The numerical results show that the RI change reflected by the shifts of resonance frequency S_1 and S_3 are different from each other. Based on this property, multiple different targets can be detected independently at the same time in this parallel scheme.

Next, to investigate the RI sensitivities of the proposed 5-channel 1D-PCNC-ISA, the device is analyzed and subjected to the variations in the bulk RI. With 3D-FDTD simulations, Fig. 8(a) shows the composed transmission spectra detected from the output port of the proposed 5-channel 1D-PCNC-ISA when all parallel-connected sensing channels are interrogated simultaneously under RI variations. It reveals that the five different resonances for sensing purpose detected at the output bus waveguide shifts towards longer wavelengths (red-shift) as the RI value is increased. In addition, each sensor is shown to independently shift its resonant peak in response to RI changes. Thus, a shift in one of them does not perturb the others. This allows the implementation of simple but functional and ultra-compact 1D-PCNC based sensor arrays, and eventually of more complex lab-on-a-chip sensor networks. Fig. 8(b) shows the observed resonant wavelength shifts as a function of the RI variations in the five parallel-connected sensors. Herein, in order to quantitatively analyze the RI sensitivities, we choose the sensitivity (S) by observing the shifts in the resonant wavelength of the sensor as a function of the RI variations, defined as $S = \Delta\lambda/\Delta n$, where $\Delta\lambda$ represents the shift of the resonant wavelength, Δn represents the RI change. From the simulation results shown in Fig. 8, the bulk RI sensitivities observed in each sensing channel (from top to bottom in y-direction (Fig. 4))

as high as $S_1 = 170.6$ nm/RIU, $S_2 = 152.7$ nm/RIU, $S_3 = 138.5$ nm/RIU, $S_4 = 128.1$ nm/RIU, and $S_5 = 120.5$ nm/RIU are obtained, respectively. Since the power confinement factor in each cavity differs from one another, their sensitivity also vary. In addition, the device footprint of the whole 5-parallel-channel 1D-PCNC-ISA, including the input bus waveguide and output bus waveguide, is as small as $\sim 7\,\mu$m $\times$ 65 μm (width by length), which is decreased by three orders of magnitude compared to the sensor arrays based on 2D-PC cavity platforms [41]–[50], without any lowering of RI-sensitivities and Q-factors.

4. Conclusion

In summary, an ultra-compact 1D photonic crystal nanobeam cavity (1D-PCNC) with small footprint ($\sim 0.5\,\mu$m $\times$ 4 μm), ultrahigh-Q ($>10^5$) and large free spectral range (FSR, $\sim$200 nm) has been shown. Based on the use of dense integrated multiple 1D-PCNCs which are placed in parallel and directly coupled between a taper-type power splitter and a S-type power combiner, a new ultra-compact on-chip multiplexed sensor array platform with a single input port and output port, which we refer to as 1D-PCNC based integrated sensor array (1D-PCNC-ISA), has been presented and analyzed. Each 1D-PCNC resonator sensor unit has a different cavity length, which makes the output transmission of the sensor array device possess multiple different resonant modes without resonance overlap. By using 3D-FDTD method, numerical simulation results demonstrate that each sensor is independently shift its resonant peak in response to changes in refractive index in the region surrounding its cavity. The resonant peaks used for sensing purpose in the output transmission are independent from each other, i.e. a shift of one of them does not affect the position of the others. The bulk RI sensitivities of $S_1 = 170.6$ nm/RIU, $S_2 = 152.7$ nm/RIU, $S_3 = 138.5$ nm/RIU, $S_4 = 128.1$ nm/RIU, and $S_5 = 120.5$ nm/RIU in the 5-channel 1D-PCNC-ISA are obtained. In addition, it is worth mentioning that the footprint of the presented ultra-compact 5-channel 1D-PCNC-ISA is $\sim 7\,\mu$m $\times$ 65 μm (width by length), decreased by three orders of magnitude compared to 2D-PC based sensor arrays. Thus, the proposed ultra-compact multi-channel 1D-PCNC-ISA in this paper is an ideal system for lab-on-chip multiplexed label-free sensing applications.

Acknowledgement

D. Yang would like to thank Dr. Anna Shneidman from the group of Prof. Marko Loncar at Harvard University for improving the English of the paper.

References

[1] R. Daw and J. Finkelstein, "Introduction Lab on a chip," *Nature*, vol. 442, pp. 367–418, 2006.
[2] H. Craighead, "Future lab-on-a-chip technologies for interrogating individual molecules," *Nature*, vol. 442, pp. 387–393, 2006.
[3] L. Novak, P. Neuzil, J. Pipper, Y. Zhang, and S. Lee, "An integrated fluorescence detection system for lab-on-a-chip applications," *Lab Chip*, vol. 7, pp. 27–29, 2007.
[4] N. A. Mortensen, S. Xiao, and J. Pedersen, "Liquid-infiltrated photonic crystals: enhanced light-matter interactions for lab-on-a-chip applications," *Microfluidics Nanofluidics*, vol. 4, pp. 117–127, 2008.
[5] W. Gao *et al.*, "Fully integrated wearable sensor arrays for multiplexed in situ perspiration analysis," *Nature*, vol. 529, pp. 509–514, 2016.
[6] Y. Zhi, X. Yu, Q. Gong, L. Yang, and Y. Xiao, "Single nanoparticle detection using optical microcavities," *Adv. Mater.*, vol. 29, no. 12, 2017, Art. no. 1604920.
[7] M. R. Foreman, J. D. Swaim, and F. Vollmer, "Whispering gallery mode sensors," *Adv. Opt. Photon.*, vol. 7, no. 2, pp. 168–240, 2015.
[8] B. B. Li, W. R. Clements, X. C. Yu, K. Shi, Q. Gong, and Y. F. Xiao, "Single nanoparticle detection using split-mode microcavity Raman lasers," *Proc. Nat. Acad. Sci. USA*, vol. 111, no. 41, pp. 14657–14662, 2014.
[9] A. Densmore *et al.*, "Silicon photonic wire biosensor array for multiplexed real-time and label-free molecular detection," *Opt. Lett.*, vol. 34, pp. 3598–3600, 2009.
[10] J. Homola, S. S. Yee, G. Gauglitz, "Surface plasmon resonance sensors: review," *Sensors Actuators B, Chem.*, vol. 54, pp. 3–15, 1999.

[11] B. K. Singh and A. C. Hillier, "Surface plasmon resonance imaging of biomolecular interactions on a grating-based sensor array," *Anal. Chem.*, vol. 78, no. 6, pp. 2009–2018, 2006.
[12] G. Zheng, F. Patolsky, Y. Cui, W. Wang, and C. M Lieber, "Multiplexed electrical detection of cancer markers with nanowire sensor arrays," *Nature Biotechnol.*, vol. 23, pp. 1294–1301, 2005.
[13] C. Wang, Y. Chang, M. Abbas, M. Shih, and D. Tsai, "T-shaped plasmonic array as a narrow-band thermal emitter or biosensor," *Opt. Exp.*, vol. 17, pp. 13526–13531, 2009.
[14] K. D. Vos *et al.*, "Multiplexed antibody detection with an array of silicon-on-insulator microring resonators," *IEEE Photon. J.*, vol. 1, no. 4, pp. 225–235, Oct. 2009.
[15] C. F. Carlborg *et al.*, "A packaged optical slot-waveguide ring resonator sensor array for multiplex label-free assays in labs-on-chips," *Lab Chip*, vol. 10, pp. 281–290, 2010.
[16] K. B. Gylfason *et al.*, "On-chip temperature compensation in an integrated slot-waveguide ring resonator refractive index sensor array," *Opt. Exp.*, vol. 18, pp. 3226–3237, 2010.
[17] M. Iqbal *et al.*, "Label-free biosensor arrays based on silicon ring resonators and high-speed optical scanning instrumentation," *IEEE J. Select. Topics Quantum Electron.*, vol. 16, no. 3, pp. 654–661, May/Jun. 2010.
[18] A. J. Qavi and R. C. Bailey, "Multiplexed detection and label-free quantitation of microRNAs using arrays of silicon photonic microring resonators," *Angew. Chemie*, vol. 49, no. 27, pp. 4608–4611, 2010.
[19] D.-X. Xu *et al.*, "Label-free biosensor array based on silicon-on-insulator ring resonators addressed using a WDM approach," *Opt. Lett.*, vol. 35, pp. 2771–2773, 2010.
[20] A. A. Eftekhar, Z. Xia, F. Ghasemi, and A. Adibi, "Ultra-Compact Multiplexed Lab-on-Chip Sensors using Miniaturized Integrated Photonic Resonators," *Proc. IEEE Photon. Conf.*, pp. 23–27 Sep. 2012.
[21] M. Mao, S. Chen, and D. Dai, "Cascaded ring-resonators for multi-channel optical sensing with reduced temperature sensitivity," *IEEE Photon. Technol. Lett.*, vol. 28, no. 7, pp. 814–817, Apr. 2016.
[22] J. Lee, S. Sung, J. Choi, S. Eom, N. Mortensen, and J. H. Shin, "Ultra sub-wavelength surface plasmon confinement using air-gap, sub-wavelength ring resonator arrays," *Sci. Rep.*, vol. 6, 2016, Art. no. 22305.
[23] R. S. Weis, A. D. Kersey, and T. A. Berkoff, "A four-element fiber grating sensor array with phase-sensitive detection," *IEEE Photon. Technol. Lett.*, vol. 6, no. 12, pp. 1469–1472, Dec. 1994.
[24] A. D. Kersey *et al.*, "Fiber grating sensors," *J. Lightw. Technol.*, vol. 15, pp. 1442–1463, 1997.
[25] S. Yun, D. J. Richardson, and B. Kim, "Interrogation of fiber grating sensor arrays with a wavelength-swept fiber laser," *Opt. Lett.*, vol. 23, pp. 843–845, 1998.
[26] C. Chan, W. Jin, H. L. Ho, and M. S. Demokan, "Performance analysis of a time-division-multiplexed fiber Bragg grating sensor array by use of a tunable laser source," *IEEE J. Select. Topics Quantum Electron.*, vol. 6, no. 5, pp. 741–749, Sep./Oct. 2000.
[27] Z. Jin and M. Song, "Fiber grating sensor array interrogation with time-delayed sampling of a wavelength-scanned fiber laser," *IEEE Photon. Technol. Lett.*, vol. 16, no. 8, pp. 1924–1926, Aug. 2004.
[28] L. Jin, Y. Liang, M. Li, L. Cheng, J. Li, and B. Guan, "A 16-element multiplexed heterodyning fiber grating laser sensor array," *J. Lightw. Technol.*, vol. 32, pp. 3808–3813, 2014.
[29] J. Arkwright, I. Underhill, S. Maunder, A. Jafari, N. Cartwright, and C. Lemckert, "Fiber optic pressure sensing arrays for monitoring horizontal and vertical pressures generated by traveling water waves," *IEEE Sensor J.*, vol. 14, no. 8, pp. 2739–2742, Aug. 2014.
[30] X. Yu *et al.*, "Single nanoparticle detection and sizing using a nanofiber pair in an aqueous environment," *Adv. Mater.*, vol. 26, no. 44, pp. 7462–7467, 2014.
[31] R. Li, C. Tian, Y. Zhang, J. Zhang, X. Chen, and S. Liu, "Simultaneous measurement of force and temperature by a multi-position fiber Loop ringdown sensor array," *J. Lightw. Technol.*, vol. 33, pp. 3607–3612, 2015.
[32] Y. Zhang, R. Li, Y. Shi, J. Zhang, X. Chen, and S. Liu, "Real time interrogation technique for fiber Bragg grating enhanced fiber loop ringdown sensors array," *Opt. Exp.*, vol. 23, pp. 14245–14251, 2015.
[33] P. Jiang, L. Ma, W. Wang, Z. Hu, and Y. Hu, "Crosstalk reduction and demodulation stability promotion in inline fiber Fabry–Pérot sensor array using phase generated carrier scheme," *J. Lightw. Technol.*, vol. 34, pp. 1006–1014, 2016.
[34] H. Y. Fu *et al.*, "Multiplexing of polarization-maintaining photonic crystal fiber based Sagnac interferometric sensors," *Opt. Exp.*, vol. 17, no. 21, pp. 18501–18512, 2009.
[35] G. A. C. Sevilla, V. Finazzi, J. Villatoro, and V. Pruneri, "Photonic crystal fiber sensor array based on modes overlapping," *Opt. Exp.*, vol. 19, pp. 7596–7602, 2011.
[36] J. Topol'anik, P. Bhattacharya, J. Sabarinathan, and P.-C. Yu, "Fluid detection with photonic crystal-based multichannel waveguides," *Appl. Phys. Lett.*, vol. 82, pp. 1143–1145, 2003.
[37] W. Lai, S. Chakravarty, Y. Zou, and R. T. Chen, "Multiplexed detection of xylene and trichloroethylene in water by photonic crystal absorption spectroscopy," *Opt. Lett.*, vol. 38, pp. 3799–3802, 2013.
[38] S. Kita, K. Nozaki, and T. Baba, "Refractive index sensing utilizing a CW photonic crystal nanolaser and its array configuration," *Opt. Exp.*, vol. 16, no. 11, pp. 8174–8180, 2008.
[39] E. Guillermain and P. M. Fauchet, "Multi-channel biodetection via resonant microcavities coupled to a photonic crystal waveguide," *Proc. SPIE*, vol. 7167, 2009, Art. no. 71670D.
[40] S. Pal, E. Guillermain, R. Sriram, B. L. Miller, and P. M. Fauchet, "Silicon photonic crystal nanocavity-coupled waveguides for error-corrected optical biosensing," *Biosensors Bioelectron.*, vol. 26, no. 10, pp. 4024–4031, 2011.
[41] D. Yang, H. Tian, and Y. Ji, "Nanoscale photonic crystal sensor arrays on monolithic substrates using side-coupled resonant cavity arrays," *Opt. Exp.*, vol. 19, no. 21, pp. 20023–20034, 2011.
[42] D. Yang, H. Tian, N. Wu, Y. Yang, and Y. Ji, "Nanoscale torsion-free photonic crystal pressure sensor with ultra-high sensitivity based on side-coupled piston-type microcavity," *Sens. Actuators A*, vol. 199, pp. 30–36, 2013.
[43] D. Yang, H. Tian, and Y. Ji, "Nanoscale low crosstalk photonic crystal integrated sensor array," *IEEE Photon. J.*, vol. 6, no. 1, 2014, Art. no. 4200107.
[44] L. Bai *et al.*, "Hybrid mesoporous colloid photonic crystal array for high performance vapor sensing," *Nanoscale*, vol. 6, pp. 5680–5685, 2014.

[45] Y. Zou, S. Chakravarty, W. Lai, C. Lin, and R. T. Chen, "Methods to array photonic crystal microcavities for high throughput high sensitivity biosensing on a silicon-chip based platform," *Lab Chip*, vol. 12, pp. 2309–2312, 2012.
[46] W. Lai, S. Chakravarty, Y. Zou, and R. T. Chen, "Silicon nano-membrane based photonic crystalmicrocavities for high sensitivity bio-sensing," *Opt. Lett.*, vol. 37, no. 7, pp. 1208–1210, 2012.
[47] S. Chakravarty *et al.*, "Multiplexed specific label-free detection of NCI-H358 lung cancer cell linelysates with silicon based photonic crystal microcavity biosensors," *Biosensors Bioelectron.*, vol. 43, pp. 50–55, 2013.
[48] Y. Zou, S. Chakravarty, L. Zhu, and R. T. Chen, "The role of group index engineering in series-connected photonic crystal microcavities for high densitysensor microarrays," *Appl. Phys. Lett.*, vol. 104, no. 14, 2014, Art. no. 141103.
[49] H. Yan *et al.*, "Silicon on-chip bandpass filters for the multiplexing of high sensitivity photonic crystal microcavity biosensors," *Appl. Phys. Lett.*, vol. 106, 2015, Art. no. 121103.
[50] D. Yang, C. Wang, W. Yuan, B. Wang, Y. Yang, and Y. Ji, "Silicon on-chip side-coupled high-Q micro-cavities for the multiplexing of high sensitivity photonic crystal integrated sensors array," *Opt. Commun.*, vol. 374, pp. 1–7, 2016.
[51] S. Arafa, M. Bouchemat, T. Bouchemat, and A. Benmerkhi, "High sensitive optofluidic sensor array based on ring-shaped holes photonic crystal H0-cavity," *Optik*, vol. 131, pp. 49–57, 2017.
[52] S. Mandal and D. Erickson, "Nanoscale optofluidic sensor arrays," *Opt. Exp.*, vol. 16, no. 3, pp. 1623–1631, 2008.
[53] D. Psaltis, S. R. Quake, and C.Yang,"Developing optofluidic technologythrough the fusion of microfluidics and optics," *Nature*, vol. 442, no. 7101, pp. 381–386, 2006.
[54] C. Monat, P. Domachuk, and B. J. Eggleton, "Integrated opto-fluidics: A new river of light," *Nature Photon.*, vol. 1, no. 2, pp. 106–114, 2007.
[55] 2017. [Online]. Available: https://en.wikipedia.org/wiki/Wavelength-division_ multiplexing
[56] Q. Quan, P. B. Deotare, and M. Loncar, "Photonic crystal nanobeam cavity strongly coupled to the feeding waveguide," *Appl. Phys. Lett.*, vol. 96, 2010, Art. no. 203102.
[57] C. Sauvan, G. Lecamp, P. Lalanne, and J. P. Hugonin, "Modal-reflectivity enhancement by geometry tuning in Photonic Crystal microcavities," *Opt. Exp.*, vol. 13, pp. 245–255, 2005.
[58] P. Lalanne and J. P. Hugonin, "Bloch-wave engineering for high-Q, small-V microcavities," *IEEE J. Quantum Electron.*, vol. 39, pp. 1430–1438, Nov. 2003.
[59] Lumerical Solutions, Inc., Vancouver, BC, Canada. [Online]. Available: http://www.lumerical.com
[60] J. D. Joannopoulos, S. G. Johnson, J. N. Winn, and R. D. Meade, *Photonic Crystals: Molding the Flow of Light*, 2nd ed. Princeton, NJ, USA: Princeton Univ. Press, 2008.
[61] P. B. Deotare, L. C. Kogos, I. Bulu, and M. Loncar, "Photonic crystal nanobeam cavities for tunable Filter and Router Applications," *Sel. Topics Quantum Electron.*, vol. 19, no. 2, 2013, Art. no. 3600210.
[62] A. R. M. Zain and B. Y. Majlis, "Reproducibility and free spectral range (FSR) control of a high quality factor-1D photonic crystal (PhC) extended cavity," in *Proc. 2015 IEEE 10th Regional Symp. Micro Nanoelectron.*, Kuala Terengganu, Malaysia, 2015, Art. no. 15664887.
[63] I. Prieto *et al.*, "Free spectral range enlargement by selective suppression of optical modes in photonic crystal L7 microcavities," in *Proc. 2015 IEEE 17th Int. Conf. Transparent Opt. Netw*, Budapest, Hungary, 2015, Art. no. 15366128.
[64] Z. Wang, N. Zhu, Y. Tang, L. Wosinski, D. Dai, and S. He, "Ultracompact low-loss coupler between strip and slot waveguides," *Opt. Lett.*, vol. 34, pp. 1498–1500, 2009.
[65] D. Yang, H. Tian, Y. Ji, and Q. Quan, "Design of simultaneous high-Q and high-sensitivity photonic crystal refractive index sensors," *J. Opt. Soc. Amer. B*, vol. 30, pp. 2027–2031, 2013.
[66] X. Chen, B. Wang, D. Yang, and Y. Ji, "A Flexible and ultracompact 1 $\times$ N optical power splitter based on tapered silicon waveguides," Optics Communications, under review (2017).
[67] S. R. Quake and A. Scherer, "From micro- to nanofabrication with soft materials," *Science*, vol. 290, pp. 1536–1540, 2000.